NANO LETTERS

Letter

pubs.acs.org/NanoLett

Enhancement of Perovskite-Based Solar Cells Employing Core–Shell Metal Nanoparticles

Wei Zhang,[†] Michael Saliba,[†] Samuel D. Stranks,[†] Yao Sun,[‡] Xian Shi,[‡] Ulrich Wiesner,[‡] and Henry J. Snaith*,[†]

[†]Department of Physics, University of Oxford, Clarendon Laboratory, Parks Road, Oxford, United Kingdom

[‡]Department of Materials Science and Engineering, Cornell University, Ithaca, New York 14853, United States

Supporting Information

ABSTRACT: Recently, inorganic and hybrid light absorbers such as quantum dots and organometal halide perovskites have been studied and applied in fabricating thin-film photovoltaic devices because of their low-cost and potential for high efficiency. Further boosting the performance of solution processed thin-film solar cells without detrimentally increasing the complexity of the device architecture is critically important for commercialization. Here, we demonstrate photocurrent and efficiency enhancement in meso-superstructured organometal halide perovskite solar cells incorporating core–shell Au@SiO_2 nanoparticles (NPs) delivering a device efficiency of up to 11.4%. We attribute the origin of enhanced photocurrent to a previously unobserved and unexpected mechanism of reduced exciton binding energy with the incorporation of the metal nanoparticles, rather than enhanced light absorption. Our findings represent a new aspect and lever for the application of metal nanoparticles in photovoltaics and could lead to facile tuning of exciton binding energies in perovskite semiconductors.

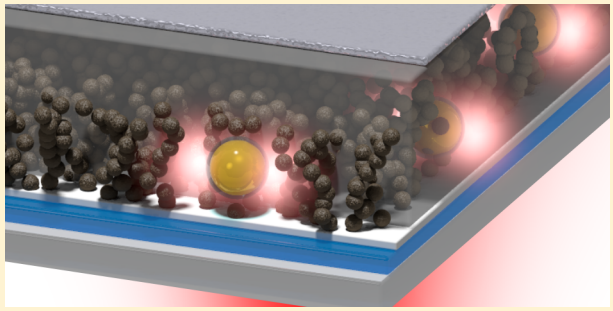

KEYWORDS: *Perovskites, thin-film solar cells, Au@SiO_2 nanoparticles, exciton binding energy, free charge carriers*

Solid-state thin film solar cells represent a promising technology to harvest and convert solar energy to electricity efficiently and cost-effectively.[1−8] There exists a plethora of technologies, ranging from thin film absorber layers of binary and tertiary semiconductor compounds,[9,10] to demixed polymer blends, where the nano to mesostructure is essential to efficiently ionize excitons (the primary excited state following light absorption) and extract charge. Very recently, organometal halide perovskites have been employed as the absorber layer in hybrid solar cells, exhibiting exceptionally low loss photovoltaic operation, as well as a simple solution based synthetic route from abundant sources (C, N, Pb, and halogen). Miyasaka and co-workers first reported a 3.8% efficient $CH_3NH_3PbI_3$ "perovskite sensitized" solar cell (PSSC), employing a liquid electrolyte in a conventional dye-sensitized solar cell (DSSC) architecture.[11] By replacing the liquid electrolyte with a solid organic hole conductor spiro-OMeTAD (2,2′,7,7′-tetrakis(*N*,*N*-di-*p*-methoxyphenylamine)-9,9′-spirobifluorene), Park and co-workers and ourselves achieved between 8 and 9.7% efficiency based on perovskite sensitized mesoporous TiO_2 devices,[4,5] and Etgar and co-workers[12] demonstrated operating mesoporous TiO_2-perovskite solar cells without any additional hole-transporter (redox couple). Meanwhile, we discovered that by removing the TiO_2 and coating a mixed-halide perovskite $CH_3NH_3PbI_{3-x}Cl_x$ on an insulating mesoporous Al_2O_3 film, device efficiencies up to 10.9% could be realized in what we term a meso-superstructured solar cell (MSSC).[5] Importantly, our results demonstrated that $CH_3NH_3PbI_{3-x}Cl_x$ can provide an efficient electron transport pathway without the need for an n-type oxide, which removes a major loss interface in the sensitized approach. More recently we have demonstrated that $CH_3NH_3PbI_{3-x}Cl_x$ can operate as a solid-thin film semiconductor, undertaking all of the roles of light absorption and effective transport of both electrons and holes in an efficient p–i–n heterojunction solar cell.[13,14] These findings demonstrate the great potential of perovskites as inexpensive and efficient absorber materials for solution-processed photovoltaics. Even though the perovskite absorbers can already absorb sun light effectively in well-operating solar cells, there are additional efficiency gains possible by enhancing the light absorption near the band edge and ensuing thinning of the solar cell. Beyond enhanced light absorption, by locally concentrating the sun light with for example metallic nanostructures, fundamental enhancements in efficiency could be achieved which could help to approach or even surpass the 1 sun Shockley–Queisser limit without any exotic operating principles.[15,16] In addition, the absorption spectrum of the active layer in the device is potentially tunable by adjusting the size and shape of metal NPs

Received: July 2, 2013
Revised: August 13, 2013
Published: August 15, 2013

   dx.doi.org/10.1021/nl4024287 | *Nano Lett.* 2013, 13, 4505–4510

introducing prospects for color tuning for aesthetic demands in building integrated photovoltaics (BIPV).

To date, several effective routes have been developed to incorporate metal NPs into solar cells, with most reports attributing enhancements to increased light absorption through plasmonic effects. In a first route, the near-field electric field enhancement of metal NPs upon surface plasmon excitation is employed to enhance the effective light absorption cross-section of a solar cell.[17−20] In a second route, light scattering off the plasmonic metal NPs is employed to redirect light into a solar cell increasing the optical path-length.[21] In a third route, metal NPs are utilized as a sensitizer directly, to harvest light and inject photoinduced electrons to an electron acceptor.[22] The latter example is arguably the clearest demonstration of a "plasmonic solar cell" to date, since there is no ambiguity as to which component is responsible for absorbing the sun light. Although plasmonic light trapping and device performance enhancements are widely reported in many systems, there are very few examples where these photocurrent enhancements can be spectrally correlated to the plasmonic light coupling. Here we incorporate Au@SiO_2 core−shell nanoparticles into perovskite based solar cells for the first time. We observe significant enhancements in photocurrent generation and efficiency, but this is *not* accounted for by enhanced light absorption. Through a photoluminescence study, we show evidence that the exciton binding energy in the perovskite absorber is reduced from 100 to 35 meV with the incorporation of Au@SiO_2 core−shell nanoparticles, which we postulate resultantly delivers enhanced free carrier generation and hence enhanced photocurrent at room temperature.

In this report, we combine core−shell metal−dielectric nanoparticles within a thin-film solar cell technology employing a recently developed perovskite absorber. The structure of the solar cells is shown schematically in Figure 1a. A 50-nm-thick, compact anatase TiO_2 layer is deposited on a conducting glass substrate to ensure selective collection of electrons at the fluorine doped tin oxide (FTO contact), which is followed by a mesoporous layer of Al_2O_3 of about 130 nm in thickness. To incorporate metal nanoparticles (NPs) into the solar cells, Au@SiO_2 core−shell NPs were added to the Al_2O_3 colloid solution at a range of concentrations prior to porous alumina film deposition. The perovskite precursor solution was then spin-coated into and onto the mesoporous layer and dried at 100 °C in air. Notably, at the present concentrations of perovskite solution (30 wt % in DMF), a capping layer of solid-perovskite film was formed on top of the mesoporous alumina.[13] Finally, a layer of p-type organic hole-conductor spiro-OMeTAD was deposited on top via spin-coating to enable selective p-type contact to the perovskite absorber, and transport of holes to the thermally evaporated silver cathode. Throughout this manuscript we will term the MSSCs incorporating the Au@SiO_2 nanoparticles "Au@SiO_2 devices", and the standard MSSCs will be termed "control" or "Al_2O_3-only" devices. The Au@SiO_2 NPs were prepared by a three-step synthesis described elsewhere.[23,24] We show a representative TEM image of a Au@SiO_2 NP in Figure 1b. The Au NPs of about 80 nm diameter are coated by an approximate 8 nm SiO_2 shell, with a absorption peak at ∼550 nm in water, as shown in Figure 1c. The slightly red-shifted extinction spectrum of Au@SiO_2 NPs as compared to that of Au NPs is expected from the change in the local refractive index which slightly shifts to longer wavelength upon addition of the silica shell.[25] As compared to bare Au NPs, we have previously shown that Au NPs with

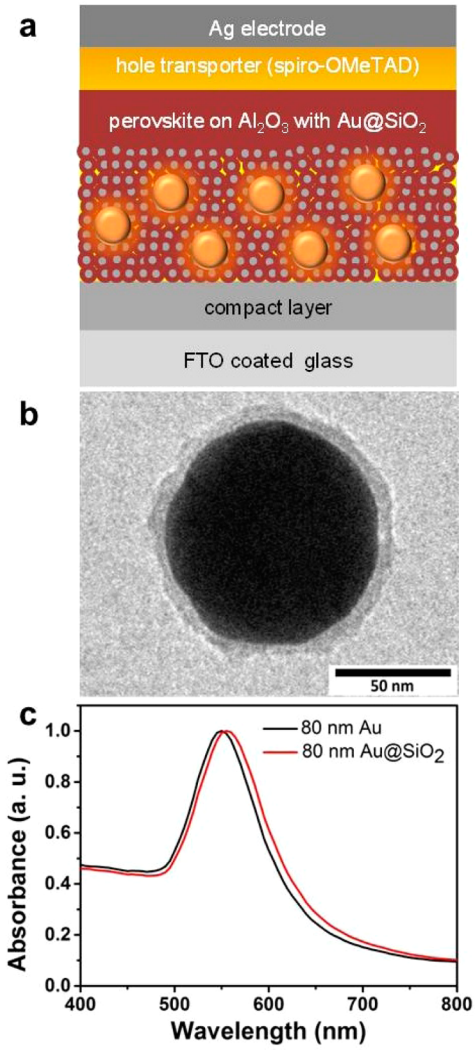

Figure 1. (a) Illustration of device structure with different components labeled. (b) TEM image of Au@SiO_2 NPs. (c) UV−vis spectra in water of parent Au as well as Au@SiO_2 NPs.

insulating SiO_2 shells have better structural and thermal stability, in particular preventing Oswald ripening and enabling thermal processing during device fabrication.[17] More importantly, the insulating SiO_2 shell prevents direct contact between Au and the hole conductor spiro-OMeTAD, or the perovskite, inhibiting an unwanted charge recombination pathway within the devices.

To investigate the effect of Au@SiO_2 NPs on device performance, we fabricated the standard MSSCs with only Al_2O_3 NPs as the scaffold and those incorporating the Au@SiO_2 NPs at 0.45−1.8 wt % (see Methods) with respect to the Al_2O_3. In Figure 2a we show the photocurrent density−voltage (J−V) curves of the MSSCs with and without the incorporation of Au@SiO_2 NPs with the same film thickness. The Al_2O_3-only device has a peak power conversion efficiency (PCE) of 10.7%, whereas the Au@SiO_2 device exhibited a PCE of 11.4%. Compared with the Al_2O_3-only device, the fill factor (FF) and open-circuit voltages (V_{oc}) were similar, while the short-circuit current density (J_{sc}) significantly increased from 14.8 to 16.9 mA/cm^2. We further investigated the effect of Au@SiO_2 concentration on device performance. In Figure 2b we show the average device performance parameters as the concen-

dx.doi.org/10.1021/nl4024287 | *Nano Lett.* 2013, 13, 4505−4510

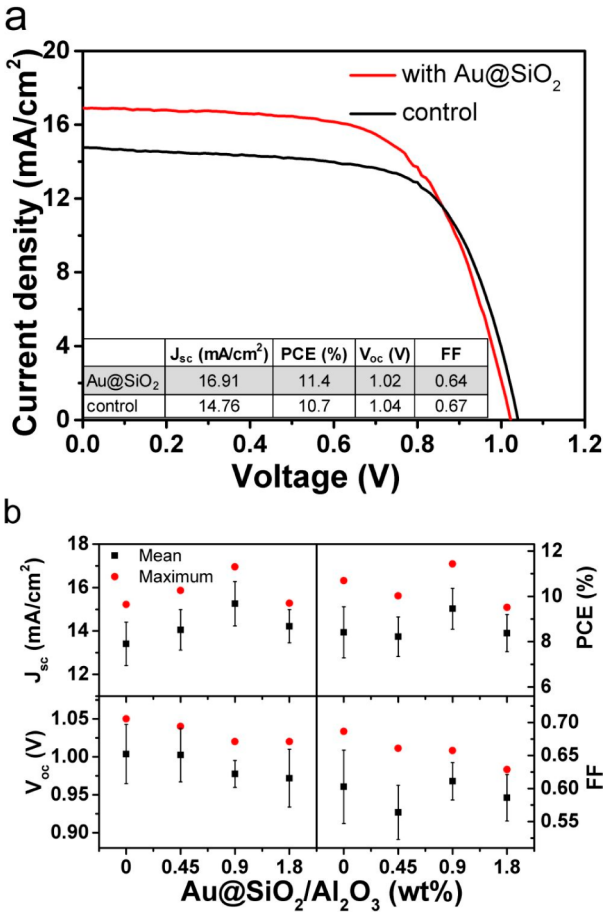

Figure 2. (a) Representative $J-V$ curves for Al_2O_3-only and Au@SiO_2 devices measured under AM1.5 simulated sunlight (100 mW/cm^2 irradiance). (b) Concentration dependence of Au@SiO_2 NPs on the device performance as measured over 48 devices for each concentration.

tration of Au@SiO_2 NPs varies from 0 to 1.8 wt %. To ensure reliability, 48 devices were made for each concentration. At the optimum concentration of 0.9 wt %, an average PCE of 9.5% was achieved, which is 13% higher than the average control device efficiency of 8.4%. In addition, the average J_{sc} increased by 13.5% from 13.4 to 15.3 mA/cm^2. Therefore, we can confidently conclude that incorporation of Au@SiO_2 NPs has improved the device performance by enhancing the photocurrent.

To confirm that the improvement of device performance is due to the effect of Au core rather than the possible scattering enhancements or another electronic influence of the SiO_2 shell, we performed a control experiment by incorporating SiO_2 NPs (~100 nm in diameter) into the Al_2O_3 paste. Considering the density difference for Au (d = 19.30 g/cm^3) and SiO_2 (d = 2.648 g/cm^3), the concentration of SiO_2 NPs was correspondingly tuned from 0 to 0.24 wt %. Both, the J_{sc} and PCE decreased when SiO_2 NPs were incorporated (shown in Supporting Information, Figure S1). Therefore, we attribute the enhancement of J_{sc} and PCE for the Au@SiO_2 devices to the presence of the Au core rather than to any effect from the SiO_2 shell.

To demonstrate broader applicability of this approach, we also fabricated devices based on a mesoporous TiO_2 layer, where the device represents a "perovskite sensitized solar cell", and results are shown in Supporting Information, Figure S2. A similar enhancement trend is obtained for both J_{sc} (increased from 12.7 to 13.7 mA/cm^2) and PCE (increased from 6.0 to 7.2%) when Au@SiO_2 NPs are incorporated into TiO_2.

We emphasize that we have observed this trend of enhanced photocurrent over tens of sets of devices over a period of more than 12 months of experimentation. As initially designed, we would expect to be able to attribute the improvement in enhanced photocurrent to enhanced light harvesting through plasmonic light interaction in the metal nanoparticles. However, we have carefully measured the light absorption in the films, and plasmon enhanced light absorption cannot be justified: In Figure 3a, we show the absorptance of the active

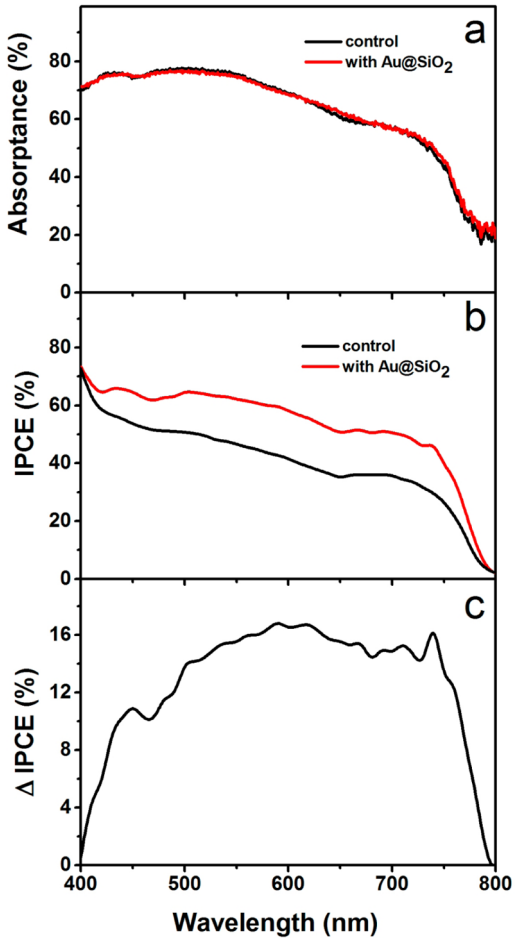

Figure 3. (a) Absorptance of the active layer in Al_2O_3-based device without (control) and with Au@SiO_2 NPs. (b) IPCE spectra of control and Au@SiO_2 devices. (c) The increase in IPCE (ΔIPCE) with the addition of Au@SiO_2 NPs.

layer in complete MSSCs (including Ag back electrode) with and without Au@SiO_2 NPs, as measured by reflectance spectroscopy in an integrating sphere, accounting for light absorption in the FTO. The light absorption in the Au@SiO_2 device is indistinguishable from the control. This is due to the low loading of Au@SiO_2 NPs (0.9 wt %) in the Al_2O_3 film. In Figure 3b we show the incident photon-to-current conversion efficiency (IPCE) for typical devices. The IPCE spectrum from the Au@SiO_2 device is increased over the whole wavelength range (400–750 nm), as compared to the control device. Based on Figure 3b, we further calculate the increase in IPCE

dx.doi.org/10.1021/nl4024287 | Nano Lett. 2013, 13, 4505–4510

(ΔIPCE) with the addition of the Au@SiO_2 NPs, which we show in Figure 3c. Although there are some features in the spectrum, the enhancement is broadly distributed over the whole range and does not specifically follow the plasmon mode profile. We note that a bias white light of ∼50 mW/cm^2 was present during the IPCE measurements.

We unambiguously observe enhanced photocurrent, but no significant change to the light harvesting capability. SiO_2 nanoparticles on their own do not enhance the photocurrent, but rather reduce it. Thus our conclusion is that Au@SiO_2 NPs enhance the solar cells internal conversion efficiency. Following light absorption, the enhancement of which we have ruled out, the improvement could either be due to enhanced charge separation/free carrier generation or due to enhanced charge collection. To probe the charge transport and recombination and hence any changes to the charge collection in the complete solar cells, we performed transient photocurrent and photovoltage decay measurements on the perovskite sensitized solar cells (the transport in the MSSCs is too fast to make quantitative analysis with our experimental setup). We observed negligible differences in both transport and recombination with the incorporation of the Au@SiO_2 NPs (shown in Supporting Information, Figure S3), indicating that they are not the cause for the enhanced photocurrent.

To probe any early time changes to the primary exciton or electron−hole pairs in the perovskite absorber, we performed a series of time-resolved and steady state photoluminescence (PL) measurements on perovskite-coated mesoporous alumina, with and without the addition of Au@SiO_2 NPs. We note that spiro-OMeTAD was not present in these films. Figure 4a shows

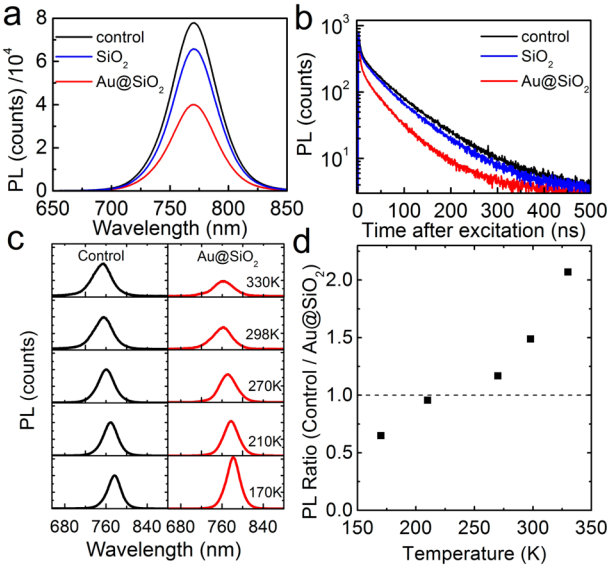

Figure 4. Photoluminescence study. (a) Time-integrated spectra and (b) time-resolved PL decays (detected at 765 nm), averaged across measurements from 16 samples, for perovskite coated on Al_2O_3-only (control) and films incorporating SiO_2 or Au@SiO_2 NPs. (c) Temperature dependence of time-integrated PL spectra for perovskite films coated on Al_2O_3-only (control) and films incorporating Au@SiO_2 NPs. The spectra for the controls have been normalized to the peak of the emission, and the films incorporating Au@SiO_2 NPs scaled accordingly. We note that both samples exhibit a considerable increase in absolute PL on reducing temperature (see Supporting Information). (d) Ratio of the wavelength integrated PL of the control and sample incorporating Au@SiO_2 NPs.

the room temperature time-integrated PL spectra, averaged across 16 samples, revealing a significant reduction in the PL of the perovskite samples incorporating Au@SiO_2 NPs. The time-resolved measurements at the peak perovskite emission (765 nm) are shown in Figure 4b. Again we observe an enhanced PL quenching rate with the Au@SiO_2 NPs, with global biexponential fits to the 16 measurements giving time constants of τ_1 = 4.88 ± 0.66 ns and τ_2 = 71.25 ± 1.45 ns for the control (no Au@SiO_2 NPs) and shorter values of τ_1 = 3.48 ± 0.41 ns and τ_2 = 50.94 ± 1.32 ns for the perovskite films coated on the mesoporous alumina scaffold containing the Au@SiO_2 NPs. By contrast, there is only a slight change in the PL decay dynamics and time-integrated spectra with the addition of solid SiO_2 NPs at a similar concentration.

These results show that the presence of the metal nanoparticles quenches the photoluminescence at room temperature. If we were dealing with a system incorporating tightly bound Mott excitons, such as organic semiconductors, we would assume that the excitons are being quenched by either energy transfer to the metal nanoparticles, a speeding up of the radiative or nonradiative decay rate, or via induced charge separation. Judging by the enhanced photocurrent in the devices, energy transfer to the metal nanoparticles is unlikely, and speeding up of the nonradiative or radiative decay rate is also unlikely to result in enhanced charge generation. Hence we would conclude that ionization of the exciton and enhanced charge separation is occurring. With the perovskite system, the binding energy of the exciton has been reported to be ∼50 meV,[26] which should exhibit more delocalized Wannier-like exciton characteristics. However, this has only been estimated on $CH_3NH_3PbI_3$ in the low temperature orthorhombic phase, and if the exciton binding energy of our material here is larger, there may be coexistence of excitons and free charge and a certain fraction of geminate electron−hole recombination at room temperature, which would result in photoluminescence.

To probe the influence of the Au@SiO_2 NPs in more depth, we have performed a temperature-dependent study of the photoluminescence. As shown in Figure 4c and the Supporting Information Figure S5, on reducing temperature the photoluminescence increases in magnitude considerably, likely to be due to an increased fraction of excitonic recombination,[27] and also undergoes a red-shift. The red-shift with reducing temperature is unusual for *conventional semiconductors* but has been previously reported for Pb-based compounds which exhibit a negative Varshni parameter.[28−30] One means to determine the exciton binding energy in conventional semiconductors,[31,32] which has been employed many times previously for semiconducting perovskites,[27,33] is to measure the absolute PL quenching of the exciton emission as a function of temperature, where the exciton PL from a material with a low exciton binding energy is rapidly quenched with increasing temperature, and a system with a larger exciton binding energy is more gradually quenched with increasing temperature. As can be seen in Figure 4c, the PL from the sample incorporating Au@SiO_2 NPs is considerably larger than that of the control at 170 K, but lesser in magnitude than the control at room temperature. Plotting the ratio of the wavelength-integrated PL intensity for the Au@SiO_2 samples over the control samples (Figure 4d), we observe a steep gradient, going from just above 0.5 at low temperatures, to just above 2 at high temperatures.

First, the enhanced PL in the samples incorporating Au@SiO_2 NPs at low temperature indicates that the presence of the Au@SiO_2 nanoparticles is not enhancing any nonradiative

dx.doi.org/10.1021/nl4024287 | *Nano Lett.* 2013, 13, 4505−4510

recombination processes and, by contrast, result in a speeding up of the radiative decay rate.[34] If we make the assumption that the majority of the PL is originating from radiative exciton recombination, then we can use these data to estimate the exciton binding energy for the two systems (shown in Supporting Information, Figure S6).[27,33] By fitting the integrated PL we determine exciton binding energies of ∼98 meV for the control samples, which drops to ∼35 meV for the samples incorporating Au@SiO_2 NPs. The reduction in exciton binding energy in the proximity of surface plasmon modes has been previously demonstrated for Al-coated ZnO,[35] but to the best of our knowledge, never observed before in any photovoltaic system. This is strong evidence for reduced exciton binding energy in the studied perovskite absorber with the incorporation of the core−shell metal nanoparticles and consistent with the solar cell characteristics. However, we note that our results rely on the assumption that the PL is predominately from exciton recombination. Although this has been applied previously for similar perovskites, it requires more detailed and extensive measurements of the fundamental exciton and charge dynamics in this largely uninvestigated perovskite semiconductor to ultimately conclude. The precise mechanism which is responsible for reducing the exciton binding energy is also not fully understood and requires further experimental and theoretical investigation but is likely to be due to the subtleties of exciton−plasmon coupling.[34] We also note that we observe a slight red-shift in PL position for the Au@SiO_2 samples in comparison to the control films, which becomes more apparent at lower temperatures. We would expect to observe a blue-shift with reduced binding energy for a conventional semiconductor, since the exciton absorption should be just below the band gap. However, at these relatively high temperatures, thermal broadening may mask these effects.

Another possible enhancement mechanism which has been proposed in the literature for other solar cells is plasmonic heating where local heating of the metal nanoparticles due to light absorption could result in improved operation of the solar cell due to increased temperature.[36] However, if this was the predominant influence, we would expect both PL quenching and a corresponding blue-shift at any given temperature, which we do not observe. We would also expect to see some spectral signature mapping the absorption of the nanoparticles in the spectral response of the device. We do note again, however, that a white light bias is used, which may mask this effect.

In summary, we have developed a successful strategy for incorporating core−shell metal-dielectric NPs into organometal halide perovskite solar cells. At optimized conditions, the Au@SiO_2 device exhibited a significantly enhanced short-circuit photocurrent (J_{sc}) and average PCE of 9.5% as compared to the control device which showed an average PCE of 8.4%. Interestingly, at the optimum concentrations of Au@SiO_2 nanoparticles, the light absorption in the complete devices is not significantly enhanced. Through a time-resolved and steady state temperature-dependent photoluminescence study, we attribute the origin of the improved J_{sc} to a reduced exciton binding energy, and hence enhanced generation of free charge carriers with the incorporation of the metal nanoparticles. This represents a new enhancement mechanism for metal nanoparticles incorporated into photovoltaics and may prove to be exceptionally useful for this new family of perovskite semiconductors where the exciton binding energy is in the order of 100 meV. We do note, however, that further work is required to fully understand the mechanism which is driving the enhanced solar cell performance.

■ ASSOCIATED CONTENT

Supporting Information

Method details, additional device performance, charge transport and recombination study, and photoluminescence spectra. This material is available free of charge via the Internet at http://pubs.acs.org.

■ AUTHOR INFORMATION

Corresponding Author

*E-mail: h.snaith1@physics.ox.ac.uk.

Author Contributions

W.Z. and M.S. contributed equally to this work. H.J.S. and U.W. supervised the study. W.Z. fabricated the devices and contributed to major characterization techniques. M.S. contributed to material characterization, device characterization, and simulation work. S.D.S. contributed to the PL measurements and analysis. Y.S. and X.S. contributed to the synthesis and characterization of Au@SiO_2 NPs. All authors provided input to data analysis, discussed the results, and assisted in manuscript preparation.

Notes

The authors declare no competing financial interest.

■ ACKNOWLEDGMENTS

The authors acknowledge financial support from EPSRC, the SUPERGEN SuperSolar project, the World Gold Council and the ERC through the ERC StG HYPER (project no. 279881). The work was further supported by the National Science Foundation (NSF) through the Materials World Network grant between the US (DMR-1008125) and the UK (Engineering and Physical Sciences Research Council, EPSRC). The authors thank Dr. J. Zhang for the synthesis of SiO_2 nanoparticles, Dr. J. M. Ball for helpful discussion, and S. M. Hein for the TOC design.

■ ABBREVIATIONS

NPs, nanoparticles; DSSC, dye-sensitized solar cell; MSSC, meso-superstructured solar cell; BIPV, building integrated photovoltaics; spiro-OMeTAD, 2,2′,7,7′-tetrakis (*N*,*N*-di-*p*-methoxyphenylamine)-9,9′-spirobifluorene; PCE, power conversion efficiency; J_{sc}, short-circuit current density; FF, fill factor; V_{oc}, open-circuit voltages; IPCE, incident photon-to-current conversion efficiency; PL, photoluminescence

■ REFERENCES

(1) Sargent, E. H. *Nat. Photonics* **2012**, *6* (3), 133−135.
(2) Ip, A. H.; Thon, S. M.; Hoogland, S.; Voznyy, O.; Zhitomirsky, D.; Debnath, R.; Levina, L.; Rollny, L. R.; Carey, G. H.; Fischer, A.; Kemp, K. W.; Kramer, I. J.; Ning, Z. J.; Labelle, A. J.; Chou, K. W.; Amassian, A.; Sargent, E. H. *Nat. Nanotechnol.* **2012**, *7* (9), 577−582.
(3) Tang, J.; Kemp, K. W.; Hoogland, S.; Jeong, K. S.; Liu, H.; Levina, L.; Furukawa, M.; Wang, X. H.; Debnath, R.; Cha, D. K.; Chou, K. W.; Fischer, A.; Amassian, A.; Asbury, J. B.; Sargent, E. H. *Nat. Mater.* **2011**, *10* (10), 765−771.
(4) Kim, H. S.; Lee, C. R.; Im, J. H.; Lee, K. B.; Moehl, T.; Marchioro, A.; Moon, S. J.; Humphry-Baker, R.; Yum, J. H.; Moser, J. E.; Gratzel, M.; Park, N. G. *Sci. Rep.* **2012**, *2*, 591.
(5) Lee, M. M.; Teuscher, J.; Miyasaka, T.; Murakami, T. N.; Snaith, H. J. *Science* **2012**, *338* (6107), 643−647.

(6) Noh, J. H.; Im, S. H.; Heo, J. H.; Mandal, T. N.; Seok, S. I. *Nano Lett* **2013**, *13* (4), 1764−1769.
(7) Zhu, R.; Jiang, C.-Y.; Liu, B.; Ramakrishna, S. *Adv. Mater.* **2009**, *21* (9), 994−1000.
(8) Li, G.; Zhu, R.; Yang, Y. *Nat. Photonics* **2012**, *6* (3), 153−161.
(9) Wu, X. Z. *Sol. Energy* **2004**, *77* (6), 803−814.
(10) Katagiri, H.; Jimbo, K.; Maw, W. S.; Oishi, K.; Yamazaki, M.; Araki, H.; Takeuchi, A. *Thin Solid Films* **2009**, *517* (7), 2455−2460.
(11) Kojima, A.; Teshima, K.; Shirai, Y.; Miyasaka, T. *J. Am. Chem. Soc.* **2009**, *131* (17), 6050−6051.
(12) Etgar, L.; Gao, P.; Xue, Z. S.; Peng, Q.; Chandiran, A. K.; Liu, B.; Nazeeruddin, M. K.; Gratzel, M. *J. Am. Chem. Soc.* **2012**, *134* (42), 17396−17399.
(13) Ball, J. M.; Lee, M. M.; Hey, A.; Snaith, H. J. *Energy Environ. Sci.* **2013**, *6* (6), 1739−1743.
(14) Liu, M.; Johnston, M. B.; Snaith, H. J. *Nature* **2013**, DOI: 10.1038/nature12509.
(15) Shockley, W.; Queisser, H. J. *J. Appl. Phys.* **1961**, *32* (3), 510−519.
(16) Atwater, H. A.; Polman, A. *Nat. Mater.* **2010**, *9* (3), 205−213.
(17) Brown, M. D.; Suteewong, T.; Kumar, R. S. S.; D'Innocenzo, V.; Petrozza, A.; Lee, M. M.; Wiesner, U.; Snaith, H. J. *Nano Lett.* **2011**, *11* (2), 438−445.
(18) Standridge, S. D.; Schatz, G. C.; Hupp, J. T. *J. Am. Chem. Soc.* **2009**, *131* (24), 8407−8409.
(19) Yang, J.; You, J.; Chen, C.-C.; Hsu, W.-C.; Tan, H.-r.; Zhang, X. W.; Hong, Z.; Yang, Y. *ACS Nano* **2011**, *5* (8), 6210−6217.
(20) Wang, D. H.; Kim, D. Y.; Choi, K. W.; Seo, J. H.; Im, S. H.; Park, J. H.; Park, O. O.; Heeger, A. J. *Angew. Chem., Int. Ed.* **2011**, *50* (24), 5519−5523.
(21) Catchpole, K. R.; Polman, A. *Opt. Express* **2008**, *16* (26), 21793−21800.
(22) Reineck, P.; Lee, G. P.; Brick, D.; Karg, M.; Mulvaney, P.; Bach, U. *Adv. Mater.* **2012**, *24* (35), 4750−4755.
(23) Ziegler, C.; Eychmuller, A. *J. Phys. Chem. C* **2011**, *115* (11), 4502−4506.
(24) Graf, C.; Vossen, D. L. J.; Imhof, A.; van Blaaderen, A. *Langmuir* **2003**, *19* (17), 6693−6700.
(25) Rodriguez-Fernandez, J.; Pastoriza-Santos, I.; Perez-Juste, J.; de Abajo, F. J. G.; Liz-Marzan, L. M. *J. Phys. Chem. C* **2007**, *111* (36), 13361−13366.
(26) Ishihara, T. *J. Lumin.* **1994**, *60*−*1*, 269−274.
(27) Chen, Z.; Yu, C. L.; Shum, K.; Wang, J. J.; Pfenninger, W.; Vockic, N.; Midgley, J.; Kenney, J. T. *J. Lumin.* **2012**, *132* (2), 345−349.
(28) Lian, H. J.; Yang, A.; Thewalt, M. L. W.; Lauck, R.; Cardona, M. *Phys. Rev. B* **2006**, *73* (23), 233202.
(29) Olkhovets, A.; Hsu, R. C.; Lipovskii, A.; Wise, F. W. *Phys. Rev. Lett.* **1998**, *81* (16), 3539−3542.
(30) Ashcroft, N. W.; Mermin, N. D. *Solid State Physics*; Brooks Cole: Stamford, CT, 1976.
(31) Varshni, Y. P. *Physica* **1967**, *34* (1), 149−154.
(32) Leroux, M.; Grandjean, N.; Beaumont, B.; Nataf, G.; Semond, F.; Massies, J.; Gibart, P. *J. Appl. Phys.* **1999**, *86* (7), 3721−3728.
(33) Kitazawa, N.; Aono, M.; Watanabe, Y. *J. Phys. Chem. Solids* **2011**, *72* (12), 1467−1471.
(34) Achermann, M. *J. Phys. Chem. Lett.* **2010**, *1* (19), 2837−2843.
(35) Fang, Y. J.; Wang, Y. W.; Gu, L.; Lu, R.; Sha, J. *Opt. Express* **2013**, *21* (3), 3492−3500.
(36) Liu, W.; Lin, F.; Yang, Y.; Huang, C.; Gwo, S.; Huang, M. H.; Huang, J. *Nanoscale* **2013**, *5*, 7953−7962.